Numerical Analysis of *H*-Plane Waveguide Junctions by Combination of Finite and Boundary Elements

KIYOSHI ISE AND MASANORI KOSHIBA, SENIOR MEMBER, IEEE

Abstract—A new numerical method is formulated for the analysis of *H*-plane waveguide junctions with arbitrary cross sections. The junctions are loaded with arbitrarily shaped dielectric or ferrite. The method is a combination of the finite-element method and the boundary-element method where the finite-element method and the boundary-element method are applied to the regions with and without dielectric or ferrite, respectively. To show the validity and usefulness of the method, a lossy dielectric post and a ferrite slab in a rectangular waveguide are investigated in detail, and the computed results are compared with earlier theoretical and experimental results.

I. INTRODUCTION

A SIGNIFICANT number of studies on scattering by the obstacles in a waveguide have been reported for many years. Marcuvitz's *Waveguide Handbook* [1] describes the equivalent circuit parameters for inductive obstacles and dielectric posts in a rectangular waveguide. Leviatan, Li *et al.* [2], [3], and Auda and Harrington [4] have studied inductive posts and diaphragms in a rectangular waveguide by the moment method. Vahldieck *et al.* [5] have given the design for a metal insert filter by the method of field expansion into eigenmodes.

Nielsen [6] by the modal expansion method, Araneta [7] by adding one more terms in the variational expressions given by Schwinger, and Sahalos and Vafiadis [8] by a method similar to Nielsen's [6] using not a rectangular interaction region but a circular one have dealt with the discontinuity problem of a circular cylindrical dielectric post centered in a rectangular waveguide. Hsu and Auda [9] and Leviatan and Sheaffer [10] have by the moment method given analyses of homogeneous dielectric posts of arbitrary shape, size, location, and number, lossy as well as lossless in a rectangular waveguide. Arndt *et al.* [11], [12] have designed dielectric-slab-filled waveguide phase shifters by the method of field expansion into eigenmodes.

Davies [13] has by the modal expansion method proposed an analysis for a symmetrical waveguide junction circulator with a circular ferrite post. Okamoto [14] has by the method based on integral equations analyzed waveguide junctions with arbitrarily shaped ferrite posts. Uher *et al.* [15] have designed ferrite-slab-loaded waveguide nonreciprocal phase shifters by the method of field expansion into eigenmodes.

Recently, Koshiba *et al.* [16], [17], Webb and Parihar [18], and Lee and Cendes [19] have by the finite-element method (FEM) analysed the *H*-plane waveguide junctions. The FEM is very useful for arbitrarily shaped discontinuities including inhomogeneous and anisotropic media. However, it requires large computer memory and long computation time to solve the final matrix equation. More recently, Kagami and Fukai [20], and Koshiba and Suzuki [21] have by the boundary-element method (BEM) analysed *H*-plane waveguide junctions. The BEM is one of the "boundary" type methods based on the integral equation method. It is therefore possible to reduce the matrix dimension and to use computer memory more economically compared with a "domain" type method, such as the FEM. However, the BEM cannot be effectively applied to a problem involving inhomogeneous and anisotropic media.

This paper presents a new combination of numerical methods for the solution of scattering of *H*-plane waveguide junctions with arbitrary cross sections where junctions are allowed to be loaded with dielectric or ferrite of arbitrary shape, size, and location, lossy as well as lossless. This approach is a combination of the finite and boundary element methods (CFBEM). The waveguide junction is divided into two regions. One is the inhomogeneous region with dielectric or ferrite, and the other is the homogeneous region without dielectric or ferrite. The finite-element and boundary-element methods are applied to the inhomogeneous and homogeneous regions, respectively. The finite-element can be combined with the boundary-element on the common nodal points because these two methods are discretized in the same way. Also, analytical solutions are used for the uniform waveguides connected to the junctions.

Discontinuity problems with a large homogeneous region or with variations of the location of an inhomogeneous region can be efficiently treated by the CFBEM. To show the validity and usefulness of this method, a lossy dielectric post and a ferrite slab in a rectangular waveguide are investigated in detail, and the computed results are compared with earlier theoretical and experimental results.

Manuscript received December 31, 1987; revised April 21, 1988.

The authors are with the Department of Electronic Engineering, Hokkaido University, Sapporo, 060 Japan.

IEEE Log Number 8822156.

0018-9480/88/0900-1343$01.00 ©1988 IEEE

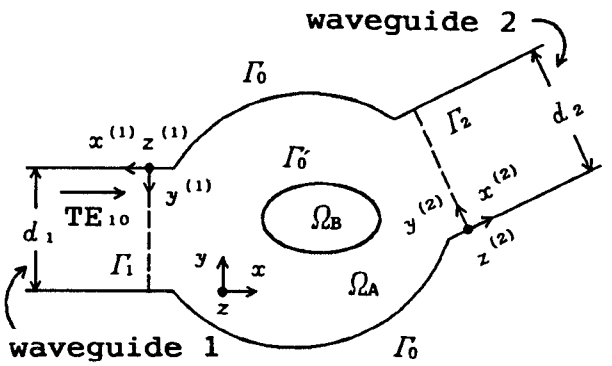

Fig. 1. H-plane waveguide junction.

Mei [22] has proposed a unimoment method in which the finite-difference or finite-element method is used together with integral equations or harmonic expansions. However, it seems that this method has not been fully applied to waveguide junctions with inhomogeneous and anisotropic media.

II. Basic Equations

We consider the waveguide junction shown in Fig. 1. Here the boundary Γ_i connects the discontinuities to the rectangular waveguide $i(i=1,2)$, d_i is the width of the waveguide for the H-plane junction, Γ_0' encloses the dielectric or ferrite region Ω_B, the region Ω_A is the one surrounded by Γ_1, Γ_2, Γ_0', and the short-circuit boundary Γ_0, and the region surrounded by Γ_1, Γ_2, and Γ_0 encloses the waveguide discontinuities completely. Besides, the dielectric or ferrite is assumed to be of full height and to be uniform along the z axis.

For a dc magnetic field H_0 in the z direction, the permeability tensor for ferrite takes on the form [17]

$$[\mu]=\mu_0\begin{bmatrix}\mu & -j\kappa & 0\\ j\kappa & \mu & 0\\ 0 & 0 & 1\end{bmatrix} \tag{1}$$

where

$$\mu=1+\frac{(\omega_0+j\omega\alpha)\omega_m}{(\omega_0+j\omega\alpha)^2-\omega^2} \tag{2}$$

$$\kappa=-\frac{\omega\omega_m}{(\omega_0+j\omega\alpha)^2-\omega^2} \tag{3}$$

$$\omega_0=\gamma H_0 \tag{4}$$

$$\omega_m=\gamma M_s/\mu_0 \tag{5}$$

$$\alpha=\gamma\Delta H/2\omega. \tag{6}$$

Here ω is the angular frequency, μ_0 is the permeability of free space, M_s is the saturation magnetization, ΔH is the resonance linewidth, and γ is the gyromagnetic ratio. A time dependence $\exp(j\omega t)$ is assumed.

Considering the excitation by the dominant TE_{10} mode, we have the following basic equations for the field E_z, H_x, and H_y because the fields do not vary with the z axis [17]:

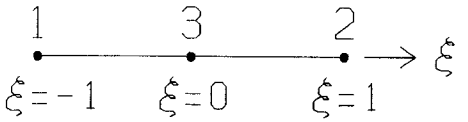

Fig. 2. Quadratic line element.

$$\frac{\partial H_y}{\partial x}-\frac{\partial H_x}{\partial y}=j\omega\epsilon_0\epsilon E_z \tag{7}$$

$$H_x=\frac{1}{j\omega\mu_0(\mu^2-\kappa^2)}\left\{-\mu\frac{\partial E_z}{\partial y}+j\kappa\frac{\partial E_z}{\partial x}\right\} \tag{8}$$

$$H_y=\frac{1}{j\omega\mu_0(\mu^2-\kappa^2)}\left\{\mu\frac{\partial E_z}{\partial x}+j\kappa\frac{\partial E_z}{\partial y}\right\} \tag{9}$$

where

$$\epsilon=\epsilon'-j\epsilon''. \tag{10}$$

Here ϵ_0 is the permittivity of free space and ϵ is the relative permittivity.

III. Mathematical Formulation

A. Boundary-Element Approach for Ω_A

For $\epsilon=1$, $\mu=1$, and $\kappa=0$ in the region Ω_A, from (7)–(9) we obtain the following Helmholtz equation:

$$\left(\frac{\partial^2}{\partial x^2}+\frac{\partial^2}{\partial y^2}\right)\phi+k_0^2\phi=0 \tag{11}$$

where ϕ is E_z and $k_0^2=\omega^2\epsilon_0\mu_0$.

Applying the boundary-element method with the quadratic line element shown in Fig. 2 to the region Ω_A, the following matrix equation is obtained [20], [21]:

$$\begin{aligned}[[H]_1\ \ [H]_2\ \ [H]_{0'}\ \ [H]_0]&\begin{bmatrix}\{\phi\}_1^A\\ \{\phi\}_2^A\\ \{\phi\}_{0'}^A\\ \{\phi\}_0^A\end{bmatrix}\\ &=[[G]_1\ \ [G]_2\ \ [G]_{0'}\ \ [G]_0]\begin{bmatrix}\{\psi\}_1^A\\ \{\psi\}_2^A\\ \{\psi\}_{0'}^A\\ \{\psi\}_0^A\end{bmatrix}\end{aligned} \tag{12}$$

where ψ is $\partial E_z/\partial n$, i.e., the outward normal derivative of E_z, and the subscripts 1, 2, 0′, and 0 denote the quantities corresponding to the boundaries Γ_1, Γ_2, Γ_0', and Γ_0 in Fig. 1, respectively.

B. Finite-Element Approach for Ω_B

Dividing the region Ω_B into a number of element subdomains Ω_e's as shown in Fig. 3, using a Galerkin procedure on (7) over the element Ω_e, and considering the contribu-

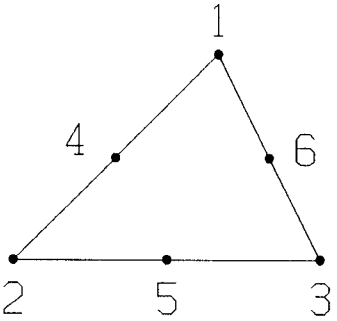

Fig. 3. Quadratic triangular element.

tion of all elements, we obtain the following matrix equation [16]–[19]:

$$[A]\{\phi\}^B = [B]_{0'}\{\psi\}^B_{0'} \tag{13}$$

$$[A] = \sum_e \iint_e \frac{1}{\mu^2-\kappa^2}\Big[\mu\big(\{N_x\}\{N_x\}^T + \{N_y\}\{N_y\}^T\big) + j\kappa\big(\{N_x\}\{N_y\}^T - \{N_y\}\{N_x\}^T\big) - k_0^2\epsilon\{N\}\{N\}^T\Big]\,dx\,dy \tag{14}$$

$$[B]_{0'} = \sum_{e'} \int_{e'} \{N\}\{N\}^T d\Gamma \tag{15}$$

where $\{N\}$ is the shape function vector, $\{N_x\} \equiv \partial\{N\}/\partial x$, $\{N_y\} \equiv \partial\{N\}/\partial y$, T denotes a transpose, $\iint_e dx\,dy$ is carried over the element subdomain Ω_e, $\int_{e'} d\Gamma$ is carried over the element contour Γ_e' on Γ_0', and Σ_e and $\Sigma_{e'}$ extend over all elements Ω_e's and the elements related to Γ_0', respectively.

Equation (13) may be rewritten as follows:

$$\begin{bmatrix} [A]_{0'0'} & [A]_{0'1'} \\ [A]_{1'0'} & [A]_{1'1'} \end{bmatrix} \begin{bmatrix} \{\phi\}^B_{0'} \\ \{\phi\}^B_{1'} \end{bmatrix} = \begin{bmatrix} [B]_{0'}\{\psi\}^B_{0'} \\ \{0\} \end{bmatrix} \tag{16}$$

where $[A]_{0'0'}, \cdots, [A]_{1'1'}$ are the submatrices of $[A]$, and $\{0\}$ is a null vector. The components of the $\{\phi\}^B_{0'}$ vector are the values of the electric field E_z at nodal points on the boundary Γ_0', and the components of the $\{\phi\}^B_{1'}$ vector are the values of E_z at nodal points in the interior region except the boundary Γ_0' from the region Ω_B.

Eliminating $\{\phi\}^B_{1'}$ from (16), we obtain the following equation:

$$[A]_{0'}\{\phi\}^B_{0'} = [B]_{0'}\{\psi\}^B_{0'} \tag{17}$$

$$[A]_{0'} = [A]_{0'0'} - [A]_{0'1'}[A]^{-1}_{1'1'}[A]_{1'0'}. \tag{18}$$

C. Analytical Approach for the Waveguides

Assuming that the dominant TE_{10} mode of unit amplitude is incident from waveguide $j(j=1,2)$ in Fig. 1, $\phi(\equiv E_z)$ on $\Gamma_i(i=1,2)$ may be expressed analytically as [21]

$$\phi\big(x^{(i)}=0,\ y^{(i)}\big) = 2\delta_{ij}f_{i1}\big(y^{(i)}\big) - \sum_m \frac{1}{j\beta_{im}}\int_0^{d_i} f_{im}\big(y^{(i)}\big)f_{im}\big(y_0^{(i)}\big) \cdot \psi\big(x^{(i)}=0,\ y_0^{(i)}\big)\,dy_0^{(i)} \tag{19}$$

where

$$f_{im}\big(y^{(i)}\big) = \sqrt{2/d_i}\,\sin m\pi y^{(i)}/d_i, \qquad m=1,2,3,\cdots \tag{20}$$

$$\beta_{im} = \sqrt{k_0^2 - (m\pi/d_i)^2}, \qquad m=1,2,3,\cdots \tag{21}$$

and δ_{ij} is the Kronecker delta function.

Equation (19) can be discretized as follows:

$$\{\phi\}^A_i - [Z]_i\{\psi\}^A_i = \delta_{ij}\{f\}_i \tag{22}$$

where

$$\{f\}_i = 2\{f_1\}_i \tag{23}$$

$$[Z]_i = -\sum_m (1/j\beta_{im})\{f_m\}_i \sum_{e'}\int_{e'} f_{im}\big(y_0^{(i)}\big) \cdot \big\{N\big(x^{(i)}=0, y_0^{(i)}\big)\big\}^T dy_0^{(i)}. \tag{24}$$

Here the components of the $\{f_m\}_i$ vector are the values of $f_{im}(y^{(i)})$ at the nodal points on Γ_i, and $\Sigma_{e'}$ extends over the elements related to Γ_i.

D. Combination of Finite and Boundary Elements

On the short-circuit boundary Γ_0, the electric-field component ϕ parallel to it vanishes, so that the following boundary condition is taken:

$$\{\phi\}^A_0 = \{0\} \qquad \text{on } \Gamma_0. \tag{25}$$

The continuity conditions of ϕ and its outward normal derivative ψ at the interface Γ_0' between regions Ω_A and Ω_B are expressed as

$$\{\phi\}^A_{0'} = \{\phi\}^B_{0'} \qquad \{\psi\}^A_{0'} = -\{\psi\}^B_{0'} \qquad \text{on } \Gamma_0' \tag{26}$$

where the minus sign of ψ originates from the outward normal direction of the adjacent two regions opposite each other.

Using (26), (17) may be expressed as

$$[A]_{0'}\{\phi\}^A_{0'} + [B]_{0'}\{\psi\}^A_{0'} = \{0\}. \tag{27}$$

Considering (25), from (12) we obtain

$$\begin{bmatrix}[H]_1 & [H]_2 & [H]_{0'}\end{bmatrix}\begin{bmatrix}\{\phi\}^A_1 \\ \{\phi\}^A_2 \\ \{\phi\}^A_{0'}\end{bmatrix} - \begin{bmatrix}[G]_1 & [G]_2 & [G]_{0'} & [G]_0\end{bmatrix}\begin{bmatrix}\{\psi\}^A_1 \\ \{\psi\}^A_2 \\ \{\psi\}^A_{0'} \\ \{\psi\}^A_0\end{bmatrix} = \{0\}. \tag{28}$$

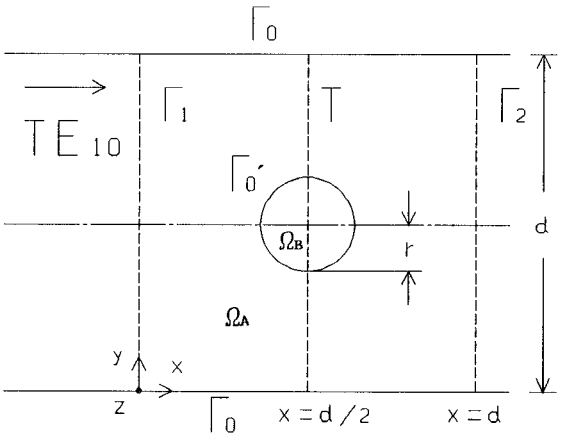

Fig. 4. Dielectric post in a rectangular waveguide.

From (22), (27), and (28) we obtain the following final matrix equation:

$$\begin{bmatrix} [1] & [0] & [0] & -[Z]_1 & [0] & [0] & [0] \\ [0] & [1] & [0] & [0] & -[Z]_2 & [0] & [0] \\ [0] & [0] & [A]_{0'} & [0] & [0] & [B]_{0'} & [0] \\ [H]_1 & [H]_2 & [H]_{0'} & -[G]_1 & -[G]_2 & -[G]_{0'} & -[G]_0 \end{bmatrix} \begin{bmatrix} \{\phi\}_1^A \\ \{\phi\}_2^A \\ \{\phi\}_{0'}^A \\ \{\psi\}_1^A \\ \{\psi\}_2^A \\ \{\psi\}_{0'}^A \\ \{\psi\}_0^A \end{bmatrix} = \begin{bmatrix} \delta_{1j}\{f\}_1 \\ \delta_{2j}\{f\}_2 \\ \{0\} \\ \{0\} \end{bmatrix} \tag{29}$$

where [1] is the unit matrix and [0] is the null matrix.

The values of ϕ at nodal points on Γ_t, i.e., $\{\phi\}_t$, are computed from (29), and then $\phi(x^{(t)}=0,\ y^{(t)})$ on Γ_t can be calculated. The solutions on Γ_t allow the determination of the scattering parameters S_{tj} of the TE_{10} mode as follows [21]:

$$S_{tt} = \int_0^{d_t} \phi\left(x^{(t)}=0,\ y^{(t)}\right) f_{t1}\left(y^{(t)}\right) dy^{(t)} - 1 \tag{30}$$

$$S_{tj} = \sqrt{\beta_{t1}/\beta_{j1}} \cdot \int_0^{d_t} \phi\left(x^{(t)}=0,\ y^{(t)}\right) f_{t1}\left(y^{(t)}\right) dy^{(t)}, \qquad i \neq j. \tag{31}$$

IV. Numerical Results

A lossy dielectric post in a rectangular waveguide as shown in Fig. 4 is investigated first, where d is the width of the rectangular waveguide and r is the radius of the cylindrical post.

The equivalent circuit for a post in a rectangular waveguide in which only the dominant TE_{10} mode can propagate unattenuated is the T network shown in Fig. 5, where Z_0 is the characteristic impedance of the TE_{10} mode.

Let S'_{11} and S'_{21} be the reflection and transmission coefficients of the dominant mode evaluated at the reference plane T ($x = d/2$ in Fig. 4), respectively. Then the

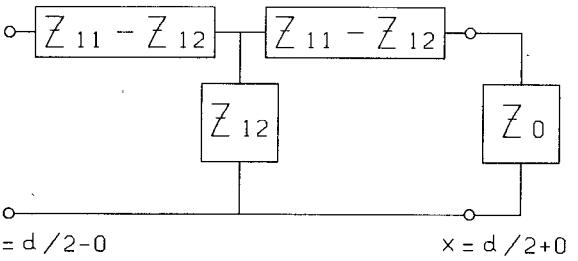

Fig. 5. Equivalent circuit for dielectric post in a rectangular waveguide.

equivalent circuit parameters are determined as follows [2]:

$$\frac{Z_{12}}{Z_0} = \frac{2S'_{21}}{(1-S'_{11}-S'_{21})(1-S'_{11}+S'_{21})}$$

$$\frac{Z_{11}-Z_{12}}{Z_0} = \frac{1+S'_{11}-S'_{21}}{1-S'_{11}+S'_{21}}.$$

Moreover the equivalent circuit parameters are represented by the resistances and reactances as follows:

$$Z_{12}/Z_0 = R_a + jX_a$$

$$(Z_{11}-Z_{12})/Z_0 = R_b + jX_b$$

where R_a and R_b are the normalized shunt and series resistances, and X_a and X_b are the normalized shunt and series reactances, respectively.

Now we take the example given by Leviatan *et al.* [10], which computes the equivalent circuit parameters as a function of ϵ'' for a centered lossy post of $r/d = 0.05$, with $\epsilon' = 4.0$ at $\lambda/d = 1.4$ ($\lambda = 2\pi/k_0$). Two limiting cases, i.e., $\epsilon'' \to 0$ and $\epsilon'' \to \infty$, correspond to the ones for the lossless post and the perfectly conducting post, respectively. Here a regular polygon with 24 sides, the area of which is equal to that of the circle, is used instead of the circle.

Figs. 6 and 7 show the normalized shunt and series resistances versus ϵ'', respectively. Figs. 8 and 9 show the normalized shunt and series reactances versus ϵ'', respectively. Fig. 10 shows the normalized total power P, i.e., $|S_{11}|^2 + |S_{21}|^2$, versus ϵ''. Our results and Leviatan's are shown by, respectively, the solid and the broken lines in these figures. Leviatan's results show the sudden change in the magnitude of each of the resistances and reactances at $\epsilon'' = 19.5$, where post losses appear to have reached a peak, and at $\epsilon'' = 60$ their results already approach the ones for

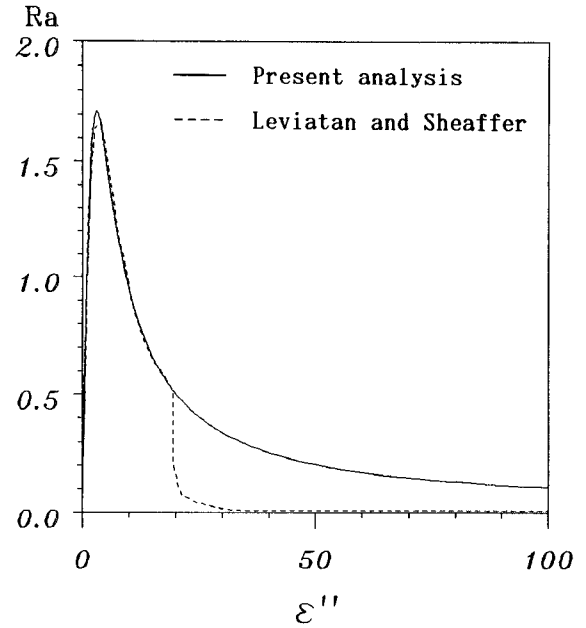

Fig. 6. Normalized shunt resistance R_a versus ϵ''.

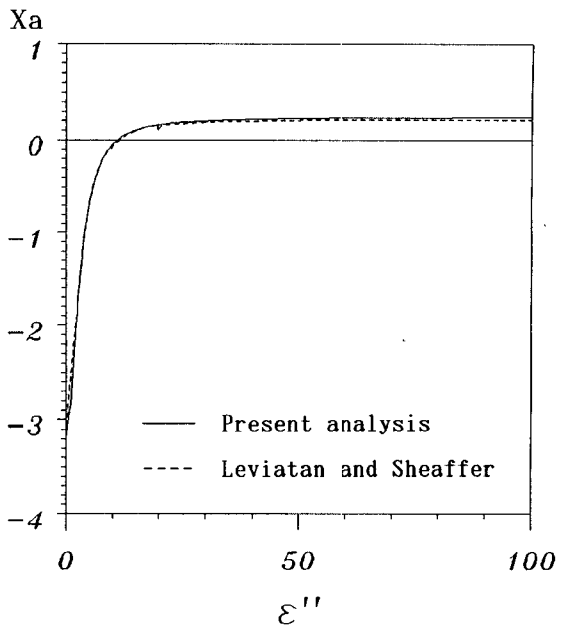

Fig. 8. Normalized shunt reactance X_a versus ϵ''.

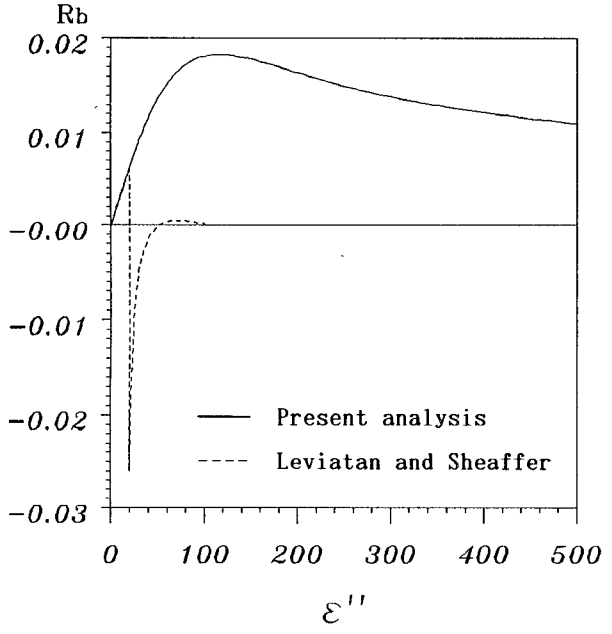

Fig. 7. Normalized series resistance R_b versus ϵ''.

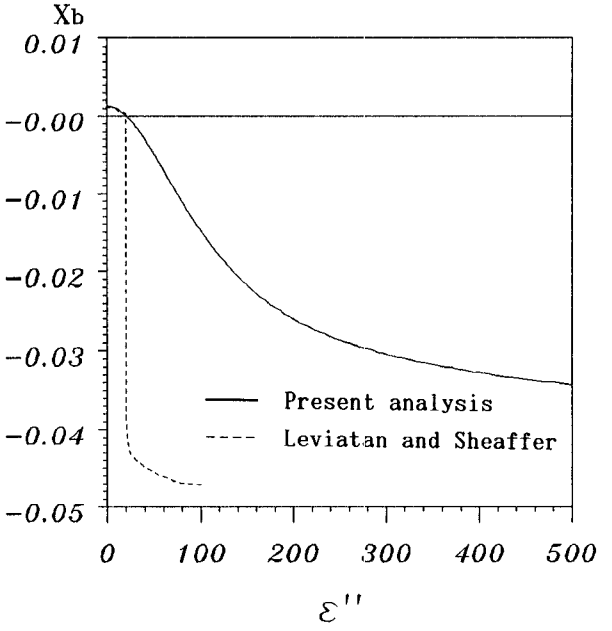

Fig. 9. Normalized series reactance X_b versus ϵ''.

the perfectly conducting post [1], i.e.,

$$R_a = 0 \qquad R_b = 0$$
$$X_a \cong 0.190 \qquad X_b \cong -0.047$$
$$|S_{11}|^2 + |S_{21}|^2 = 1.$$

Moreover, their R_b has negative values at $19.5 \leqslant \epsilon'' \leqslant 50$ although the resistor R_b should never have a negative resistance [23]. On the other hand, all of our results have no rapid changes. Some negative values for our R_b appear in Table I. This is because the total power obtained by the CFBEM becomes more than unity. Since the energy error is less than 0.06 percent, computation error seems to cause negative values for R_b. Table I shows that our results reach the ones for the perfectly conducting post at $\epsilon'' > 10^6$ and that post losses are the greatest at $\epsilon'' = 18.4$.

Marcuvitz's results [1] for the perfectly conducting post of the same volume and location as the lossy dielectric post are compared with the results obtained by the FEM or the BEM, which are shown in Table II. Our results agree well with Marcuvitz's.

From the fact described above, we may expect that our results are more reasonable than Leviatan's [10].

The computer memory and the CPU time required to analyze a lossy dielectric post in a rectangular waveguide are shown in Table III. All results obtained by the CFBEM, the FEM, and the BEM are fully convergent.

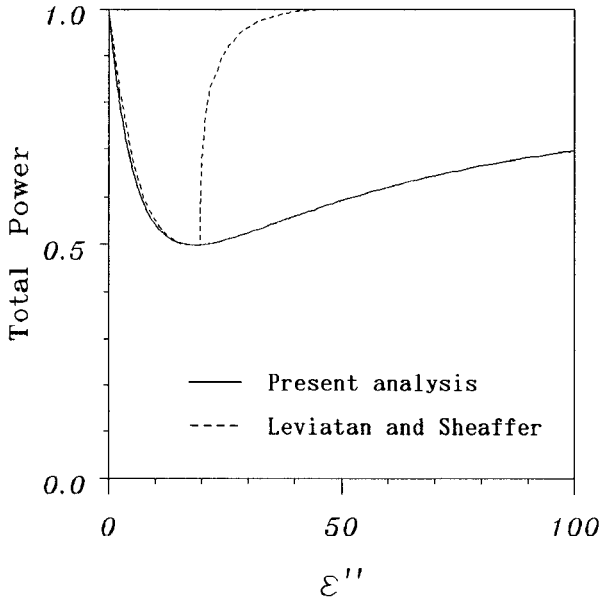

Fig. 10. Normalized total power versus ϵ''.

TABLE I
NORMALIZED RESISTANCES R_a, R_b, NORMALIZED REACTANCES X_a, X_b, AND NORMALIZED TOTAL POWER P VERSUS ϵ'' ($r/d = 0.05$, $\lambda/d = 1.4$, $\epsilon' = 4.0$)

ε''	R_a	X_a	R_b	X_b	P
0	-0.00003	-3.18718	-0.00014	0.00125	1.00029
2.9	1.70864	-1.53542	0.00082	0.00123	0.76215
3.0	1.70962	-1.47748	0.00086	0.00123	0.75626
3.1	1.70869	-1.42144	0.00089	0.00123	0.75049
11.0	0.86774	-0.00438	0.00347	0.00090	0.52950
12.0	0.80428	0.03123	0.00379	0.00083	0.52022
18.0	0.55411	0.14014	0.00567	0.00031	0.49887
18.4	0.54268	0.14403	0.00579	0.00027	0.49881
19.0	0.52637	0.14942	0.00598	0.00021	0.49892
20.0	0.50121	0.15739	0.00628	0.00010	0.49960
21.0	0.47829	0.16428	0.00658	-0.00002	0.50081
110.0	0.09762	0.23384	0.01831	-0.01649	0.70991
116.0	0.09336	0.23410	0.01833	-0.01742	0.71692
120.0	0.09079	0.23423	0.01832	-0.01801	0.72130
500.0	0.03692	0.22020	0.01099	-0.03423	0.85207
1000.0	0.02474	0.21173	0.00806	-0.03795	0.89332
10000.0	0.00770	0.19709	0.00284	-0.04413	0.96291
100000.0	0.00233	0.19091	0.00082	-0.04669	0.98864
1000000.0	0.00026	0.19027	-0.00003	-0.04697	0.99919
4000000.0	0.00006	0.19026	-0.00011	-0.04697	1.00019
10000000.0	0.00003	0.19026	-0.00013	-0.04697	1.00039
100000000.0	0.00000	0.19026	-0.00014	-0.04697	1.00051

TABLE II
NORMALIZED RESISTANCES R_a, R_b, NORMALIZED REACTANCES X_a, X_b, AND NORMALIZED TOTAL POWER P FOR A PERFECTLY CONDUCTING POST BY THE FINITE-ELEMENT METHOD AND THE BOUNDARY-ELEMENT METHOD ($r/d = 0.05$, $\lambda/d = 1.4$)

METHOD	R_a	X_a	R_b	X_b	P
FEM	-0.29×10^{-6}	0.19027	0.00002	-0.04738	0.99991
BEM	-0.40×10^{-6}	0.19026	-0.00013	-0.04697	1.00052

TABLE III
MEMORY AND CPU TIME

METHOD	MEMORY (Mbyte)	CPU TIME (s)
CFBEM	6.62	2.10
FEM	26.76	23.22
BEM	2.11	5.84

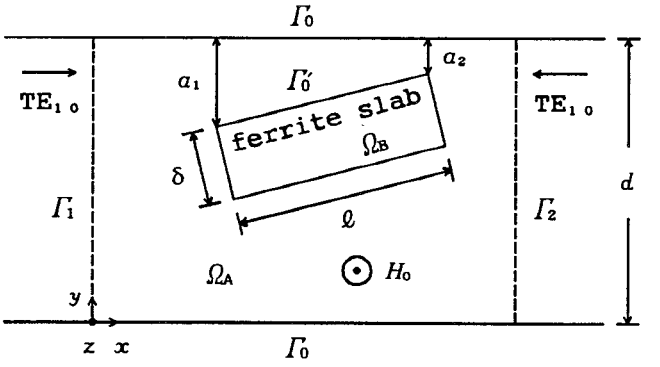

Fig 11 Ferrite slab in a rectangular waveguide.

Second, ferrite-loaded waveguide nonreciprocal phase shifters are investigated. Nonreciprocal phase shift may be realized in a rectangular waveguide by placing a ferrite slab magnetized by a dc magnetic field H_0 as shown in Fig. 11. Differential phase shift ($\Delta\phi = \arg S_{21} - \arg S_{12}$) and low *VSWR* are important to characterize the nonreciprocal phase shifter, so that phases of the forward (S_{21}) and backward (S_{12}) transmission coefficients and the amplitudes of the S parameters are obtained. Figs. 12 and 13 show, respectively, the differential phase shift and the magnitude of reflection coefficient as a function of frequency, where ferrite is TT1-2800, $H_0 = 1.2\times10^5$ A/m, $d = 15.799$ mm, $\delta = 0.7$ mm, $l = 20$ mm, and the slab is assumed to be loaded parallel to the wall and 0.7 mm distant from the wall in Fig. 11.

Our results and the experimental ones of Uher *et al.* [15] are shown by the solid and the $\times$ signs in Figs. 12 and 13, respectively. Both $\Delta\phi$'s agree well at $f > 16$ GHz, as do the $|S_{11}|$'s at $f > 16.5$ GHz, but the frequencies where the $|S_{11}|$'s take minima are different from each other.

The longer ferrite slab is dealt with, the larger the discontinuity region becomes. So that it gets more and more difficult to analyze the discontinuity region by only the FEM, because the FEM needs large memory for computation. On the other hand, the CFBEM does not need so much memory for computation, since here the FEM is applied only to the region with ferrite. For example, the computer memory required to analyze a ferrite slab ($l = 20$ mm) in a rectangular waveguide is about 7.5 Mbyte with the CFBEM, while it is a few hundred Mbyte with FEM only. So the differential phase shift $\Delta\phi$ and the magnitude of the reflection coefficient $|S_{11}|$ versus variations in the length of ferrite slab can be computed easily by the

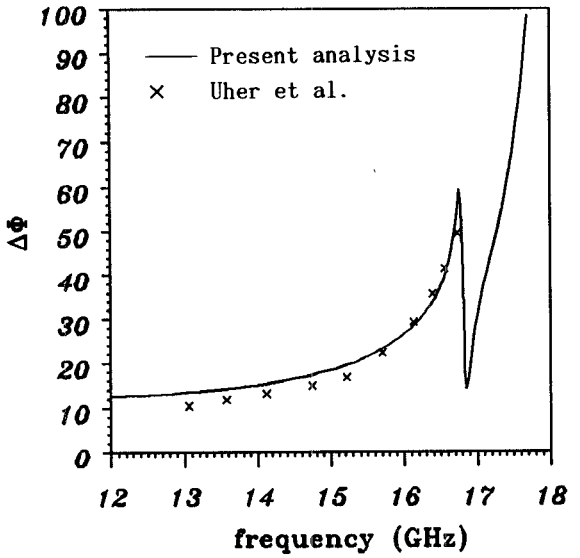

Fig. 12. Differential phase shift in degrees versus frequency ($a_1 = 0.7$ mm, $a_2 = 0.7$ mm, $\delta = 0.7$ mm, $l = 20$ mm).

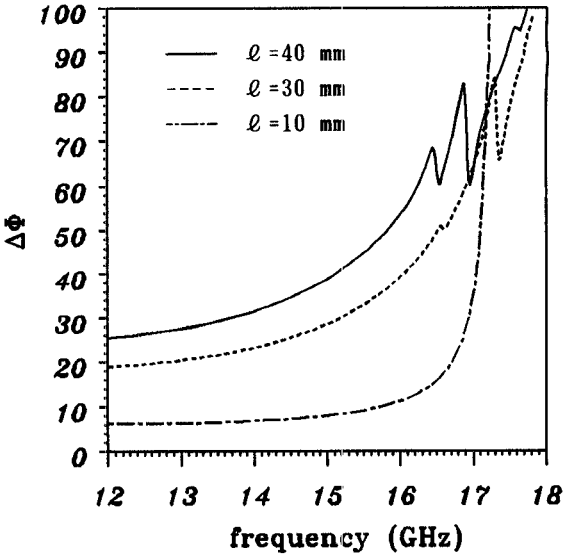

Fig. 14. Differential phase shift in degrees versus variation of length of ferrite slab ($a_1 = 0.7$ mm, $a_2 = 0.7$ mm, $\delta = 0.7$ mm).

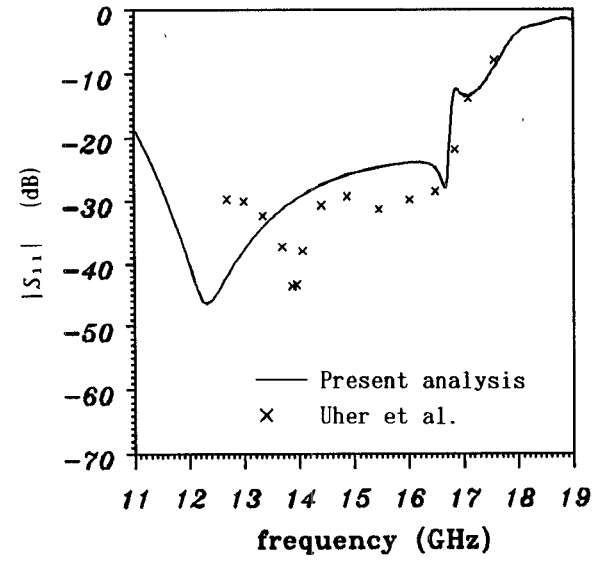

Fig. 13. Reflection coefficient in decibels versus frequency ($a_1 = 0.7$ mm, $a_2 = 0.7$ mm, $\delta = 0.7$ mm, $l = 20$ mm).

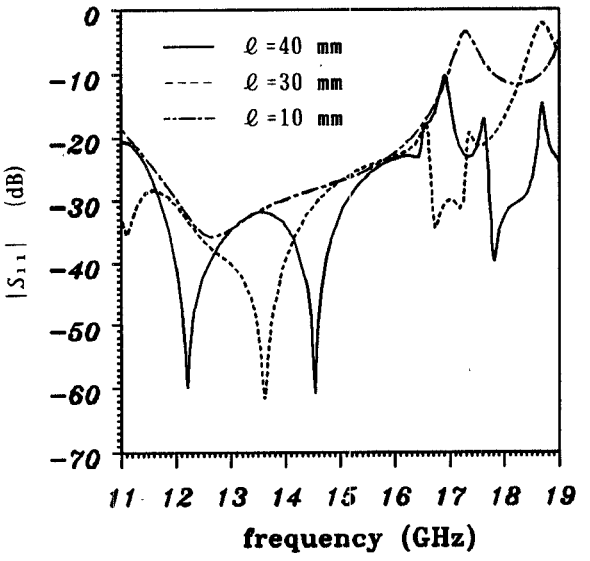

Fig. 15. Reflection coefficient in decibels versus variation of length of ferrite slab ($a_1 = 0.7$ mm, $a_2 = 0.7$ mm, $\delta = 0.7$ mm).

CFBEM. The results are shown, respectively, in Figs. 14 and 15, where $a_1 = 0.7$ mm, $a_2 = 0.7$ mm, and $\delta = 0.7$ mm in Fig. 11. As the ferrite slab is longer along the wall, more peaks of $|S_{11}|$ are seen in Fig. 15. And Table IV shows the differential phase shift by the length of a unit at $l = 10$, 20, 30, and 40 mm.

Moreover the differential phase shift obtained by a transcendental equation involving the propagation constants β_+, β_- [24] is also shown in Table IV, where magnetic losses are neglected and ferrite is assumed to be infinitely long parallel to the wall, 0.7 mm distant from the wall and $\delta = 0.7$ mm. Here let $\Delta\phi$ be $(\beta_+ - \beta_-)$. The propagation constants are difficult to obtain at $f < 12.26$ GHz because the transcendental equation has complex as well as real coefficients at $f < 12.26$ GHz in this case. And four propagation constants, i.e., two β_+'s and two β_-'s, are obtained at frequency $f > 16.36$ GHz (modal coupling can be clearly seen at $f > 16.7$ GHz in Fig. 12). In Table IV, as the ferrite slab is longer, the differential phase shift by the length of a unit seems to come near to the one obtained by a transcendental equation.

In the case where the ferrite slab is not loaded parallel to the wall, F. Arndt, J. Uher, *et al.* will treat the ferrite slab as a linearly tapered structure, which is approximated by a stepped transition with a hundred steps at each side [12]. So their method is difficult to apply to problems with variations in the angle of the ferrite slab to the wall. The CFBEM can be effectively applied even to problems with variations of the location of the ferrite slab. So the differential phase shift $\Delta\phi$ and the magnitude of the reflection coefficient $|S_{11}|$ versus the location of the ferrite slab as shown in Fig. 11 are obtained and shown in Figs. 16

TABLE IV
DIFFERENTIAL PHASE SHIFT BY THE LENGTH OF A UNIT VERSUS FREQUENCY

frequency	$\beta_+ - \beta_-$	$\Delta\phi/\ell$ (deg/mm): ℓ is length of ferrite slab			
(GHz)	(deg/mm)	ℓ=10	ℓ=20	ℓ=30	ℓ=40
11		0.65072	0.61572	0.60390	0.60176
12		0.62567	0.62793	0.62928	0.63350
12.2659	0.64204	0.62435	0.63510	0.63934	0.64507
13	0.69947	0.63302	0.66687	0.67876	0.68869
14	0.81543	0.68117	0.75092	0.77300	0.78911
15	1.00947	0.80168	0.92185	0.95028	0.97296
16	1.34641	1.12516	1.32253	1.30771	1.33855
16.3581	1.52222	1.40329	1.64663	1.53181	1.60977
17		3.46521	1.52196	2.13124	1.57972

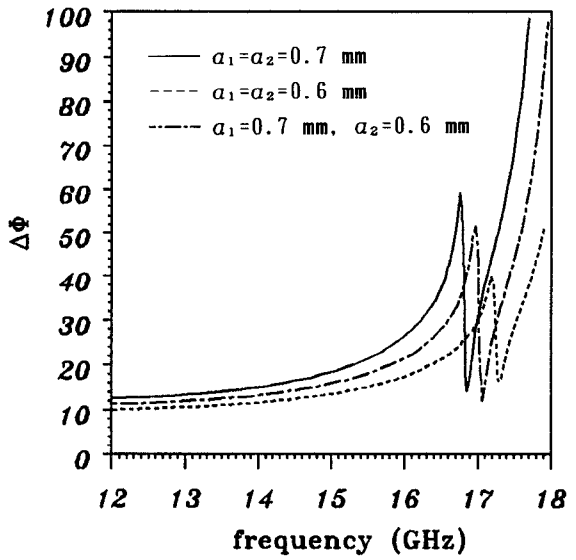

Fig. 16. Differential phase shift in degrees versus variation of location of ferrite slab ($\delta = 0.7$ mm, $l = 20$ mm).

and 17, respectively, where $\delta = 0.7$ mm and $l = 20$ mm in Fig. 11. These figures exhibit considerable differences in $\Delta\phi$'s and $|S_{11}|$'s on variations of the location of ferrite.

V. CONCLUSIONS

A combined method of the finite and boundary elements is formulated for the analysis of H-plane waveguide junction with arbitrary cross sections where the junction is loaded with dielectric or ferrite of arbitrary shape, size, and location. The waveguide junction is divided into two regions. One is the inhomogeneous region with dielectric or ferrite, and the other is the homogeneous region without dielectric or ferrite. The finite-element and the boundary-element methods are applied to the inhomogeneous and the homogeneous regions, respectively. Discontinuity problems with large homogeneous region or with variations of the location of inhomogeneous region can be effectively treated by this method. To show the validity and usefulness of the method, a lossy dielectric post in a rectangular waveguide and a ferrite-slab-loaded waveguide nonreciprocal phase shifter are investigated.

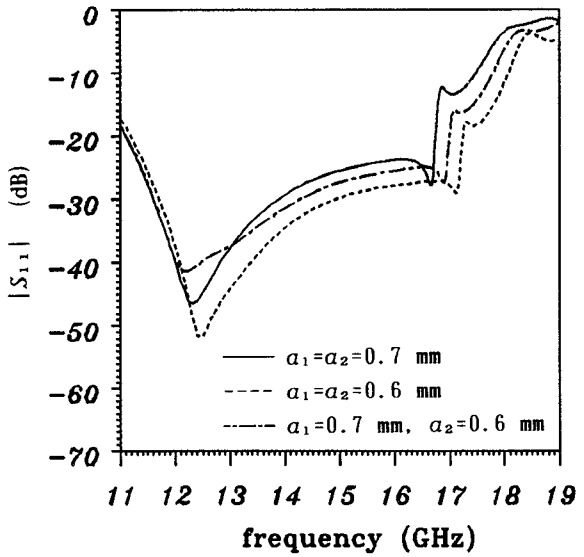

Fig. 17. Reflection coefficient in decibels versus variation of location of ferrite slab ($\delta = 0.7$ mm, $l = 20$ mm).

REFERENCES

[1] N. Marcuvitz, Ed., *Waveguide Handbook*. New York: McGraw-Hill, 1951.
[2] Y. Leviatan, P. G Li, A. T. Adams, and J. Perini, "Single-post inductive obstacle in rectangular waveguide," *IEEE Trans. Microwave Theory Tech.*, vol. MTT-31, pp 806–811, Oct. 1983.
[3] P. G Li, A. T. Adams, Y. Leviatan, and J. Perini, "Multiple-post inductive obstacle in rectangular waveguide," *IEEE Trans. Microwave Theory Tech.*, vol. MTT-32, pp. 365–373, Apr. 1984.
[4] H. Auda and R. F. Harrington, "Inductive posts and diaphragms of arbitrary shape and number in a rectangular waveguide," *IEEE Trans. Microwave Theory Tech.*, vol MTT-32, pp 606–613, June 1984.
[5] R. Vahldieck, J. Bornemann, F. Arndt, and D. Grauerholz, "W-band low-insertion-loss E-plane filter," *IEEE Trans. Microwave Theory Tech.*, vol. MTT-32, pp. 133–135, Jan. 1984.
[6] E. D. Nielsen, "Scattering by a cylindrical post of complex permittivity in a waveguide," *IEEE Trans. Microwave Theory Tech.*, vol. MTT-17, pp. 148–153, Mar. 1969.
[7] J. C Araneta, M. E Brodwin, and G. A. Kriegsmann, "High-temperature microwave characterization of dielectric rods," *IEEE Trans. Microwave Theory Tech.*, vol MTT-32, pp. 1328–1335, Oct. 1984.
[8] J. N. Sahalos and E. Vafiadis, "On the narrow-band microwave filter design using a dielectric rod," *IEEE Trans. Microwave Theory Tech* , vol. MTT-33, pp. 1165–1171, Nov. 1985
[9] C. G. Hsu and H. A. Auda, "Multiple dielectric posts in a rectangular waveguide," *IEEE Trans. Microwave Theory Tech.*, vol. MTT-34, pp. 883–891, Aug. 1986.
[10] Y. Leviatan and G. S. Sheaffer, "Analysis of inductive dielectric posts in rectangular waveguide," *IEEE Trans. Microwave Theory Tech.*, vol. MTT-35, pp. 48–59, Jan. 1987.
[11] F. Arndt, J. Bornemann, and R. Vahldieck, "Design of multisection impedance-matched dielectric-slab filled waveguide phase shifters," *IEEE Trans. Microwave Theory Tech* , vol. MTT-32, pp. 34–38, Jan. 1984.
[12] F. Arndt, A. Frye, M Wellnitz, and R. Wirsing, "Double dielectric-slab-filled waveguide phase shifter," *IEEE Trans. Microwave Theory Tech.*, vol. MTT-33, pp 373–381, May 1985.
[13] J. B. Davies, "An analysis of the m-port symmetrical H-plane waveguide junction with central ferrite post," *IRE Trans. Microwave Theory Tech* , vol. MTT-10, pp. 596–604, Nov. 1962.
[14] N. Okamoto, "Computer-aided design of H-plane waveguide junctions with full-height ferrites of arbitrary shape," *IEEE Trans. Microwave Theory Tech.*, vol MTT-27, pp 315–321, Apr. 1979.

[15] J. Uher, F. Arndt, and J. Bornemann, "Field theory design of ferrite-loaded waveguide nonreciprocal phase shifters with multisection ferrite or dielectric slab impedance transformers," *IEEE Trans. Microwave Theory Tech.*, vol. MTT-35, pp. 552–559, June 1987.

[16] M. Koshiba, M. Sato, and M. Suzuki, "Finite-element analysis of arbitrarily shaped H-plane waveguide discontinuities," *Trans. Inst. Electron. Commun. Eng. Japan*, vol. E66, pp. 82–87, Feb. 1983.

[17] M. Koshiba and M. Suzuki, "Finite-element analysis of H-plane waveguide junction with arbitrarily shaped ferrite post," *IEEE Trans. Microwave Theory Tech.*, vol. MTT-34, pp. 103–109, Jan. 1986.

[18] J. P. Webb and S. Parihar, "Finite element analysis of H-plane rectangular waveguide problems," *Proc. Inst. Elec. Eng.*, pt. H, vol. 133, pp. 91–94, Apr. 1986.

[19] J. Lee and Z. J. Cendes, "An adaptive spectral response modeling procedure for multipost microwave circuits," *IEEE Trans. Microwave Theory Tech.*, vol. MTT-35, pp. 1240–1247, Dec. 1987.

[20] S. Kagami and I. Fukai, "Application of boundary-element method to electromagnetic field problems," *IEEE Trans. Microwave Theory Tech.*, vol. MTT-32, pp. 455–461, Apr. 1984.

[21] M. Koshiba and M. Suzuki, "Application of the boundary-element method to waveguide discontinuities," *IEEE Trans. Microwave Theory Tech.*, vol. MTT-34, pp. 301–307, Feb. 1986.

[22] K. K. Mei, "Unimoment method of solving antenna and scattering problems," *IEEE Trans. Antennas Propagat.*, vol. AP-22, pp. 760–766, Nov. 1974.

[23] C. G. Hsu and H. A. Auda, "On the realizability of the impedance matrix for lossy dielectric posts in a rectangular waveguide," *IEEE Trans. Microwave Theory Tech.*, vol. MTT-36, pp. 763–765, Apr. 1988.

[24] B. K. J. Lax, K. Button, and L. M. Roth, "Ferrite phase shifters in rectangular wave guide," *J. Appl. Phys.*, vol. 25, pp. 1413–1421, 1954.

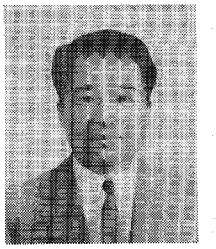

Kiyoshi Ise was born in Kinosaki, Japan, on April 7, 1954. He received the B.S. and M.S. degrees in electronic engineering from Hokkaido University, Sapporo, Japan, in 1986 and 1988, respectively. He is presently studying toward the Ph.D. degree in electronic engineering at Hokkaido University.

Mr. Ise is a member of the Institute of Electronics, Information and Communication Engineers (IEICE).

✠

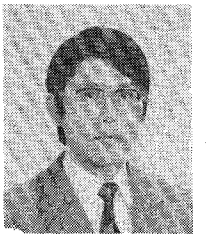

Masanori Koshiba (SM'84) was born in Sapporo, Japan, on November 23, 1948. He received the B.S., M.S., and Ph.D. degrees in electronic engineering from Hokkaido University, Sapporo, Japan, in 1971, 1973, and 1976, respectively.

In 1976, he joined the Department of Electronic Engineering, Kitami Institute of Technology, Kitami, Japan. From 1979 to 1987, he was an Associate Professor of Electronic Engineering at Hokkaido University, and in 1987 he became a Professor. He has been engaged in research on lightwave technology, surface acoustic waves, magnetostatic waves, microwave field theory, and applications of finite-element and boundary-element methods to field problems.

Dr. Koshiba is a member of the Institute of Electronics, Information and Communication Engineers (IEICE), the Institute of Television Engineers of Japan, the Institute of Electrical Engineers of Japan, the Japan Society for Simulation Technology, and the Japan Society for Computational Methods in Engineering. In 1987, he was awarded the 1986 Paper Award by the IEICE.